International Journal of Technology

http://ijtech.eng.ui.ac.id



Research Article

Optimizing Reactor Configuration and Electrode Geometry for Enhanced Electrochemical Reduction of CO₂

Pramujo Widiatmoko^{1*}, Hary Devianto¹, Silmia N. A. Irawan¹, Angela M. Vinka¹, Ira Febrianty Sukmana¹, Wibawa Hendra Saputera¹, Mitra Eviani^{1,2}, Tirto Prakoso¹

Abstract: The increasing concentration of CO₂ in the atmosphere has contributed significantly to global warming and its associated environmental effects. Electrochemical conversion has emerged as a promising approach for CO₂ capture, storage, and utilization to produce valueadded chemicals. However, the inherently low solubility of CO₂ in aqueous solutions presents a major challenge to the efficiency of process. Unlike previous studies that focused on increasing CO₂ solubility by lowering the temperature or using non-aqueous solvents, this work explores the use of smaller gas bubbles to enhance CO₂ retention time in solution. The objective is to prolong the residence time of CO₂ bubble in the electrolyte, allowing for gradual dissolution, sustained saturation, and improved interaction with the cathode surface. Under the same operating voltage, the bubble stone sparger, produces bubbles with diameters of 6.18 and 3.26-times than those generated by the atomizer and air stone, respectively, achieved 29.23% and 15.23% higher current efficiency. Similarly, the formic acid yield increased by 50.70% and 28.21%, compared to the other sparger types. The highest current efficiency (11.60%) and formic acid yield (0.122%) were obtained using the bubble stone sparger with a cathode length of 2.5 cm, a cathode-sparger distance of 0.5 cm, and an operating voltage of 6 V. These findings highlight the potential of using smaller bubble sizes to improve the electrochemical reduction of CO₂ by enhancing gas-liquid interaction and mass transfer performance.

Keywords: CO2ER; Bubble size effect; Enhance performance

1. Introduction

Global warming has demonstrated severe impacts on the environment, largely driven by the continued reliance on fossil fuels, which are the primary contributors to carbon dioxide (CO₂) emissions, the dominant greenhouse gas. In 2023, global CO₂ emissions reached 37.4 gigatons (International Energy Agency, 2024). As parts of its carbon mitigation strategy, the Indonesian government has set ambitious targets, achieving a 23% renewable energy mix by 2025 and reaching carbon neutrality by 2060, particularly in the energy sector remains heavily relies on fossil fuels (Institute for Essential Services Reform, 2021). Indonesia plans to cut 29% of CO₂ emission by 2030, with 15 CCUS project will start from 2026 (Ramadhan et al., 2024). To accelerate the process, Indonesia Ministry of Energy and Mineral has regulated the CCUS through Regulation 2/2023. The Presidential Regulation 14/2024 further expands the scope for allowing CO₂ capture in industries outside oil and gas. By 2021, a 12.77% renewable energy mix had been achieved in the power generation sector (Mudassir, 2021). Effort toward decarbonization have also been extended to other sectors such as maritime transport (Whulanza et al., 2024; Hadi et al., 2025). However, these achievements remain insufficient to meet the 2030 emissions reduction target and the 2060 net-zero target of 2060 (The International Renewable

¹Department of Chemical Engineering, Faculty of Industrial Technology, Bandung Institute of Technology, Ganesha no. 10, Bandung, West Java, 40132, Indonesia

²Center for Oil and Gas Testing, Ministry of Energy and Mineral Resources, Ciledug Raya Kav. 109, South Jakarta, 12230, Indonesia

^{*}Corresponding author: pramujo@itb.ac.id; Tel.: +62222500989

Energy Agency, 2022).

Carbon capture, utilization, and storage (CCUS) technologies aim to reduce atmospheric CO_2 concentrations. Carbon capture has been extensively applied in the oil and gas industries through technologies such as pressure swing adsorption and amine absorption. Once captured, CO_2 can be stored underground, for instance, in enhanced oil recovery operations or beneath bed rock formations. It can also be utilized in the food and beverage industries for carbonation, cooling and freezing, or inert blanketing of food products.

Among utilization pathways, converting CO₂ into value-added chemicals such as formic acid through electrochemical reduction is particularly attractive option (Irabien et al., 2018; Jia et al., 2022; Chang et al., 2023). Other target products include methane, methanol, diethyl carbonate (Anggerta et al., 2025), and ethanol have been developed. Formic acid offers several advantages: it serves as hydrogen carrier for fuel cell electric vehicles (FCEVs), is low in toxicity, and remains in liquid form under ambient conditions (Moret et al., 2014). Hydrogen can be efficiently released from formic acid at low temperatures and pressures using gold-based catalysts (Wang et al., 2018), simplifying energy storage for FCEVs. Additionally, formic acid is widely used as a reducing agent in textile dyeing to improve colorfastness and fix dyes, as a degreasing agent in leather tanning, and as a preservative in the food industry due to its antimicrobial properties. While conventional formic acid production methods such as hydrolysis, catalytic oxidation, and hydrogenation exist (Moret et al., 2014; Bulushev and Ross, 2018), electrochemical synthesis offers distinct advantages due to its mild operating condition.

Several factors influence the performance of electrochemical CO₂ reduction into formic acid, including the type of cathode (Zhu et al., 2016; Altaf et al., 2024), electrolyte composition (Fan et al., 2020; Marcandalli et al., 2022; Zhao et al., 2023), reactor design (Bagemihl et al., 2022; Ewis et al., 2023), and CO₂ concentration (Kim et al., 2015; Zhong et al., 2017). Tin-based (Sn) cathodes have demonstrated high current efficiency for CO₂ reduction (Daiyan et al., 2017), while lead (Pb) cathodes offer lower overpotential and superior durability compared to Sn (Zhao et al., 2019; Yang et al., 2020). Furthermore, KHCO₃ electrolytes have been found to yield optimal performance for formic acid production (Wu et al., 2012).

Various reactor types for CCUS, such as fixed bed, fluidized bed, slurry, membrane, and microchannel reactors have been evaluated in prior studies (G. Gao et al., 2023). This study focuses on the bubble reactor due to its simplicity, scalability, and low maintenance and operating costs (Lin et al., 2020; García and Mejia, 2021; Ewis et al., 2023; Kartohardjono et al., 2024; Madani et al., 2024). Although commonly used in wastewater treatment, its application for CCUS remains limited. Bagemihl et al., 2022 highlighted the mass transfer limitations of dissolved CO₂ in aqueous system and proposed gas-liquid Taylor flow to improve reactor performance, achieving Faradaic efficiencies over 90% at current densities up to 500 mA cm⁻² (Bagemihl et al., 2022). Factor such as film thickness and void fraction were shown to significantly affect efficiency. While Taylor flow reactors offer high mass transfer and can operate under elevated pressures, their complex flow control make them less practical for industrial use. To ensure optimal performance in bubble reactors, it is crucial to consider parameters such as bubble hold-up time and bubble diameter, which influence CO₂ diffusion into the electrolyte (Zhong et al., 2015; Angulo et al., 2020; Widiatmoko et al., 2021). Reactor dimensions including diameter, length, and the ratio of bubble to reactor diameter, also play critical roles (Temesgen et al., 2017).

The objective of this research is to identify the optimal bubble reactor configuration for converting CO_2 into formic acid by investigating the effects of sparger type, cathode length, and sparger to cathode distance. The low solubility of CO_2 in aqueous solutions is a well-known a limiting factor. To address this, smaller bubble sizes are employed to increase CO_2 retention time, thus maintaining saturation levels in the electrolyte and enhancing diffusion toward the cathode. Variations in cathode length and its distance from the sparger also affect hydrodynamic and diffusion processes. Therefore, this study aims to elucidate the effects of these parameters on the overall efficiency of the electrochemical CO_2 reduction process.

2. Methods

The experimental set up is shown in Figure 1. An H-type electrochemical cell was used, each chamber having a diameter of 5 cm and a height of 20 cm. Both chambers were filled with electrolyte to a height of 15 cm. A DC power supply provided the electrical input for electrolysis, while a voltmeter and ammeter were used to measure the applied voltage across the electrodes and the current passing through the system. The flow rate of CO_2 gas was monitored using flowmeter.

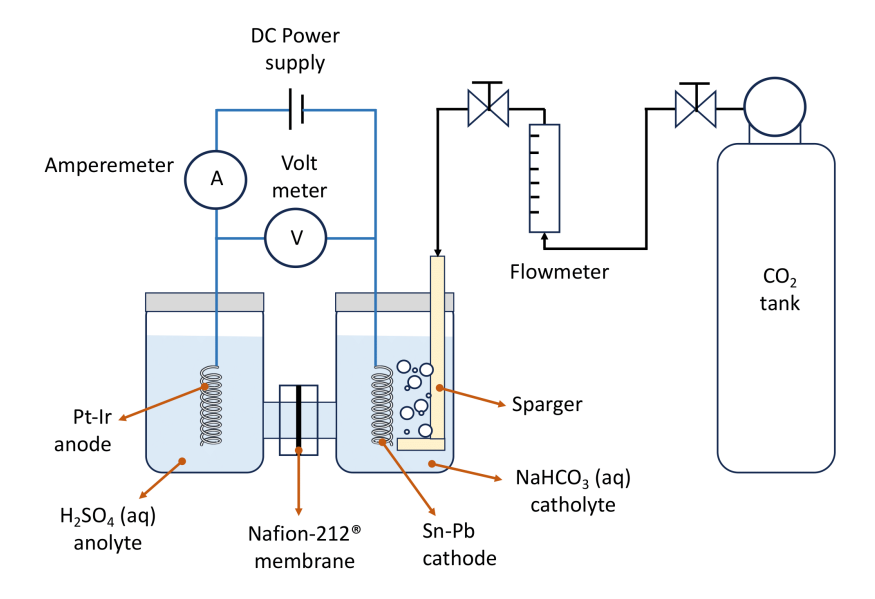


Figure 1 Schematic diagram of the experimental setup for electrochemical CO_2 reduction.

During the experiment, $\rm CO_2$ gas (99%, $\rm CV$ Sangkuriang, Indonesia) was bubbled into the reactor through a sparger, both prior to before and during electrolysis. Three types of spargers were employed: an air stone, an atomizer (Simple type D-531, Up-Aqua), and a nano bubble stone (Nano $\rm CO_2$ diffuser, Bray Deep). The bubble size distribution generated by each sparger was analyzed using an optical camera and ImageJ software, capable of detecting bubbles larger than 0.16 mm with an error margin below 10%. All reactions were carried out at atmospheric pressure (698±2 mmHg) and ambient temperature (27±3°C). The cathode consisted of a Pb-Sn alloy wire (Yosinogawa SW600688 - 40/60, 0.8 mm dia.) and the anode was a Pt-Ir alloy wire (Herman Paulsen Cat. No. AP 4-4746, 0.5 mm dia.). Both the cathode length and the distance between the cathode and the sparger were varied. A 0.5 M KHCO₃ solution was used as the catholyte and a 0.1 M H₂SO₄ solution as the anolyte. All solutions were prepared using pro-analysis grade chemicals from Merck (Germany). A Nafion 212 membrane was employed as the separator (Widiatmoko et al., 2020)

Prior to electrolysis, the catholyte was saturated with CO₂ by bubbling the gas for 1 hour. The electrolysis process was conducted for 3 hours under continuous CO₂ bubbling at a flow rate of 50 mL/min. Only upward motion of the gas bubbles cause mixing within the reactor. The cathode length was varied between 2.5 cm and 4.5 cm and the cathode-sparger distance was set at either 0.5 or 1.5 cm. This resulted in four experimental configurations: (a) 2.5 cm-0.5 cm, (b) 2.5 cm-1.5 cm, (c) 4.5 cm-0.5 cm, and (d) 4.5 cm-1.5 cm. To assess the effect of sparger type on formic acid production, experiments were conducted using different spargers while keeping the cathode length and cathode-sparger distance constant. An overpotential of 1 V was maintained across all experiments, determined from the initial current observed on the I-V curve specific to each sparger configuration.

The concentration of produced formic acid was determined by analyzing the liquid phase products using High-Performance Liquid Chromatography (Agilent PL Hi-Plex H column,

United States of America). Gas phase products were analyzed using Gas Chromatography (Shimadzu GC-2014, Japan). The morphology and surface condition of the cathode before and after electrolysis were examined using a Scanning Electron Microscope (SEM, Hitachi SU3500, Japan). X-ray diffraction (Bruker D2 phaser, Germany) was employed to identify crystalline phase and detect any structural or compositional changes on the cathode surface resulting from the electrochemical reaction.

3. Results and Discussion

3.1 Effect of CO₂ Bubble Size

CO₂ gas was introduced into the KHCO₃ catholyte by bubbling it from the bottom of reactor. Three types of spargers, i.e. air stone, atomizer, and bubble stone were used, each generating CO₂ bubbles with different sizes. The bubble size distributions are presented in Figure 2(a). The air stone produced a wide distribution of bubble sizes predominantly in the millimeter range, with a peak between 1 - 2 mm. In contrast, the atomizer and bubble stone generated bubbles in both the millimeter and sub-millimeter ranges, although with distinct distribution patterns. The atomizer exhibited two prominent peaks at approximately 0.5 mm and 1 mm, with a broader size distribution than that of the bubble stone. The bubble stone produced a narrower distribution, with a dominant peak around 0.2 mm. These sizes fall within the transition range between macrobubbles (diameter ¿ 1 mm) and microbubbles (0.001 - 1 mm). Upon release from the spargers, the bubbles tends to coalesce, forming larger bubbles due to surface tension effect.

Dissolved CO_2 is the active species in the electrochemical reduction reaction, rather than bicarbonate (HCO_3^-) or carbonate (CO_3^-) ions (Kumar et al., 2012; Fang et al., 2024). Under ambient pressure and temperature conditions, the size of CO_2 bubbles significantly influences its solubility in the catholyte solution (Bang et al., 2015), primarily due to variations in gas hold-up time. Larger CO_2 bubbles exhibit high terminal velocities, which reduce their residence time in the electrolyte and subsequently lower CO_2 dissolution (see Figure 2b). The terminal velocity of the bubbles (v) can be theoretically estimated using Stoke's Law, as shown in Equation 1.

$$v = \left(\frac{\rho fluid - \rho bubble}{\rho fluid}\right) g \frac{2}{9} r^2 \tag{1}$$

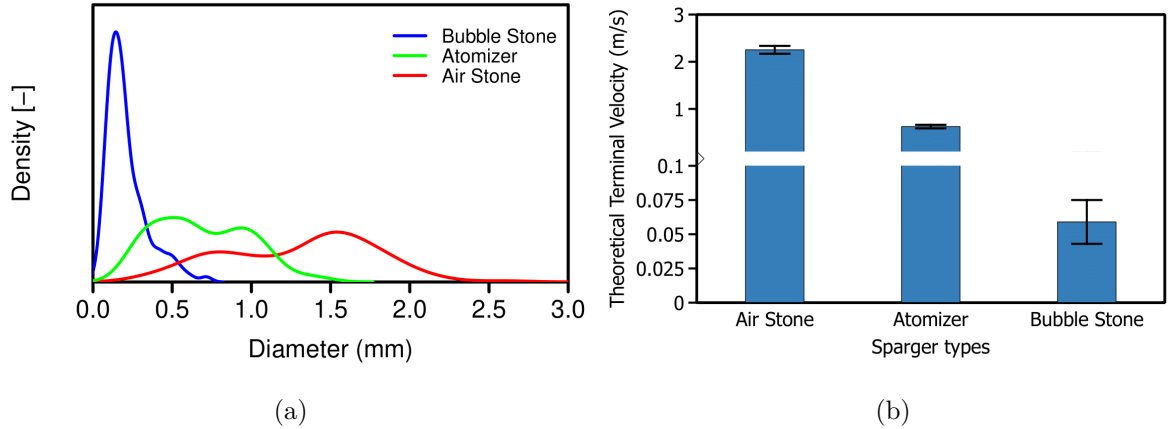


Figure 2 (a) Bubble size distribution generated by different sparger types: air stone, atomizer, and bubble stone. (b) The average theoretical terminal velocity of CO₂ bubbles produced by each sparger type, indicating differences in buoyancy-driven rise behaviour

The use of spargers that produce smaller CO_2 bubble results in lower average terminal velocity of bubbles in the catholyte solution (Temesgen et al., 2017; Widiatmoko et al., 2021). Among the sparger tested, the bubble stone produced the smallest bubbles with the lowest estimated terminal velocity of 0.059 m/s, followed by the atomizer at 0.626 m/s, and the air

stone at 2.253 m/s. Consequently, the bubble stone is expected to provide gas hold-up compared to the air stone and atomizer (Moshtari et al., 2009).

At a constant overpotential, the effect of sparger type on the activation potential becomes apparent. The observed operating voltages were 6V for the air stone, 5.6 V for the atomizer, and 5.4 V for the bubble stone. This trend shows that larger bubble sizes lead to increased operating voltage, likely due to enhanced mass transfer resistance of CO_2 at the electrode surface.

The effect of the sparger type on current efficiency under constant overpotential is presented in Figure 3. In general, the trend of formic acid yield follows that of current efficiency. While the air stone consistently shows the highest formic acid yields and the bubble stone the lowest, an exception occurs under the configuration of a 2.5 cm electrode length and a 0.5 cm sparger to electrode distance. In this case, the bubble stone delivers both higher current efficiency and yield compared to the other spargers. This indicates that smaller bubbles can enhance reaction performance but due to their low terminal velocity, diffusion is only effective at short distance. The results from the 4.5 cm-0.5 cm configuration, where the atomizer outperforms the other spargers in terms of current efficiency, supports the phenomena. The relatively larger bubbles produced by the atomizer are able to travel farther and interact more effectively along the full length of the 4.5 cm electrode. These findings shows that when employing spargers that generate smaller bubbles, the distance between the sparger and electrode must be carefully optimized to ensure effective gas diffusion and maximum electrochemical performance.

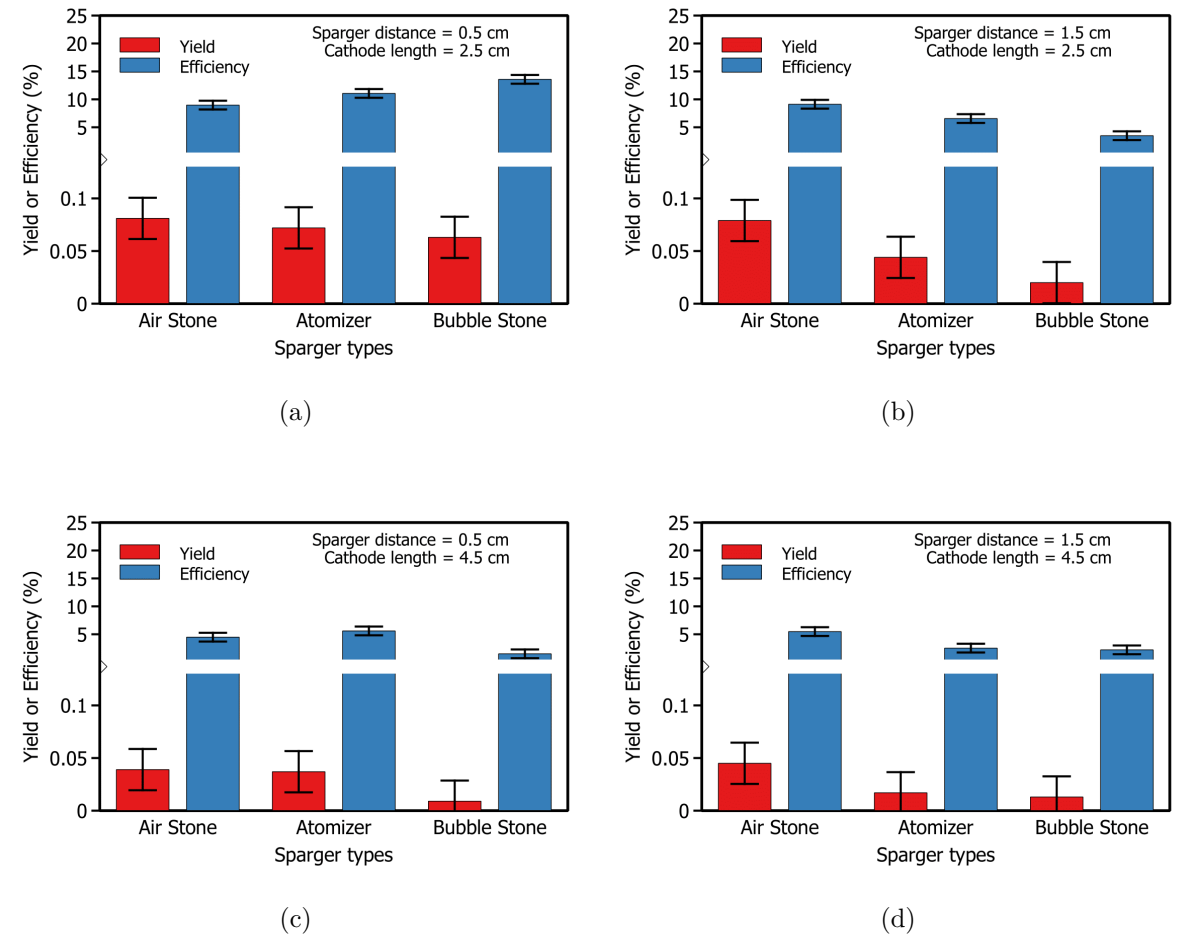


Figure 3 Effect of sparger type on current efficiency and formic acid yield at different cathode lengths and cathode-to-sparger distances Results are shown for:(a) cathode length of 2.5 cm and cathode to sparger distance of 0.5 cm (b) cathode length of 2.5 cm and cathode to sparger distance of 1.5 cm (c) cathode length of 4.5 cm and cathode to sparger distance of 0.5 cm (d) cathode length of 4.5 cm and cathode to sparger distance of 1.5 cm

3.2 Effect of Cathode Configuration

The experimental variations investigated in this study include the cathode-to-sparger distance and cathode length, both of which are expected to influence bubble-induced mass transfer. At greater distances from the cathode, larger bubbles are more likely to reach the electrode surface effectively due to their higher terminal velocity, potentially enhancing the reaction. Likewise, a longer cathode is expected to benefit from larger bubbles, as they can maintain contact over a longer vertical span. The effect of these geometric parameters on current efficiency and formic acid yield are presented in Figure 3.

Positioning the cathode closer to the sparger (0.5 cm) generally results in higher current efficiency and formic acid yield across most conditions. However, smaller bubbles tend to coalesce or break up after traveling a distance approximately equivalent to their diameter (Gemello et al., 2018). As such, increasing the sparger-to-cathode distance diminishes the advantage offered by smaller bubble size. Nevertheless, when the distance is extended to 1.5 cm, the negative impact is less significant, particularly with longer cathodes (4.5 cm), suggesting that cathode length can partially compensate for reduced CO_2 diffusion rates.

Interestingly, the use of a shorter cathode (2.5 cm) produced higher current efficiency and formic acid yield in all tested configurations compared to the 4.5 cm cathode. This result may appear counterintuitive, as a larger electrode surface area is typically expected to offer more active sites. However, area under constant applied voltage, the current density decreases with increasing electrode area, leading to less intense electrochemical reaction. Moreover, longer electrodes may suffer from uneven current distribution, further reducing their electrochemical performance (Popov et al., 2005; Bagotzky, 2006).

3.3 Effect of Bubble Size at the Same Operating Voltage

Operating the system under constant overpotential conditions resulted in different operating voltages for each sparger type. Previous studies have highlighted that precise control of applied voltage is crucial for optimizing electrochemical cell performance. Lower overpotentials typically promote the production of both formic acid and hydrogen, whereas moderate overpotentials enhance current efficiency for formic acid production, while suppressing hydrogen evolution, up to an optimum point. It has also been reported that operating voltage above 5.4 V can increase current efficiency to a certain extent (Ewis et al., 2023). To further confirm the effect of bubble size, additional experiments were conducted at a fixed operating voltage of 6 V as the highest operating voltage among variation. The results are presented in Figure 4.

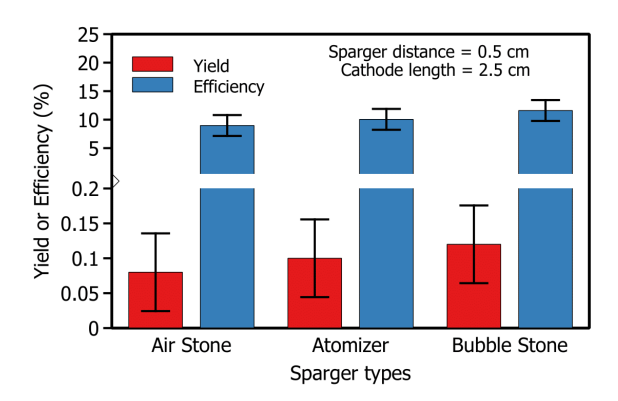


Figure 4 Effect of sparger type on current efficiency and formic acid yield under constant operating voltage of 6 V, with cathode length of 2.5 cm and a cathode-to-sparger distance of 0.5 cm. Red bars represents formic acid yield, while blue bars indicate current efficiency

The findings indicate a clear trend, both current efficiency and formic acid yield increase with decreasing bubble size, with the bubble stone sparger showing the best performance. Smaller bubbles exhibit excellent mass transfer characteristics due to their increased surface

area and the tendency for enhanced breakage and dissolution within the liquid phase (Baumgartner et al., 2023). The relationship between mass transfer and bubble size has been reported in several models (Temesgen et al., 2017; Suwartha et al., 2020). Specifically, mass transfer efficiency is govern by the specific surface area between the gas and liquid phases, which is influenced by the bubble volume and diameter (Sacco et al., 2019; Bagemihl et al., 2022). Furthermore, smaller bubble diameters are associated with higher surface tension, leading to the shrinking of micro- and nanobubbles and an increase in internal bubble pressure (Liu and Tang, 2019). These combined effects enhance CO_2 dissolution and availability at the electrode surface. Based on these observations, there remains significant potential to further improve electrochemical performance in bubble reactors by reducing the bubble size into the nanometer range.

Table 1 shows the selectivity of the electrochemical reaction using different sparger types. Under identical conditions, including cathode length, cathode-to-sparger distance, and operating voltage, the bubble stone demonstrates superior performance. Specifically, it yields a 29.23% and 15.23% increase in current efficiency, and a 50.70% and 28.21% increase in formic acid yield compared to the air stone and atomizer, respectively. These findings support the hypothesis that smaller bubble sizes can enhance the CO₂ reduction reaction, particularly by improving gas diffusion in the catholyte and maintaining the solubility of CO₂ (Widiatmoko et al., 2020).

When compared with previously reported values in the literature (see Table 2), the Faradaic efficiency achieved in this study remains relatively low. This is likely due to the limited CO_2 hold up time in the electrolyte. It is therefore proposed that design of reactor should be further optimized to intensify gas-electrode contact. Future studies will explore the use of 3D-structured cathodes and side-mounted spargers to enhance gas diffusion and utilization.

Table 1	Product	Selectivity	and CO	$_2$ Conv	version .	Efficiency	Using	Different	Sparger	Types

Parameter	\mathbf{Unit}	Air Stone	Atomizer	Bubble Stone
Product Selectivity				
- HCOOH	%	92.45	91.53	94.38
- H ₂	%	0.14	0.59	0.55
- CO	%	7.42	7.88	5.07
CO ₂ Conversion	%	23.07	26.47	32.56

Table 2 Comparison of CO₂-to-Formic Acid Conversion from Selected Studies

Method	Cathode Material	Faradaic Effeciency (FE, %)	Yield (%)	Selectivity (%)	Ref.
Bubble reactor	Pb-Sn	11.60	0.122	92.45	This work
Three-electrode	Sn	63.00	-	-	Wu et al., 2012
- Unspecified	MOF	90.50	-	-	Jia et al., 2022
Solid state reactor	nBuLi-Bi	95.00	-	-	Fan et al., 2020
Filter press reactor	Sn	70.00	-	-	Ewis et al., 2023

3.4 Morphological Analysis

The surface of the Pb-Sn alloy cathodes before and after use are presented in Figure 5. Noticeable differences in color and texture are observed following the reaction. The initially shiny surface of fresh cathode becomes visibly darker and rougher after use. This transformation is attributed to the formation of an oxide layer on the cathode surface. Despite difference in bubble conditions, all three cathodes exhibit a similar change in surface appearance.

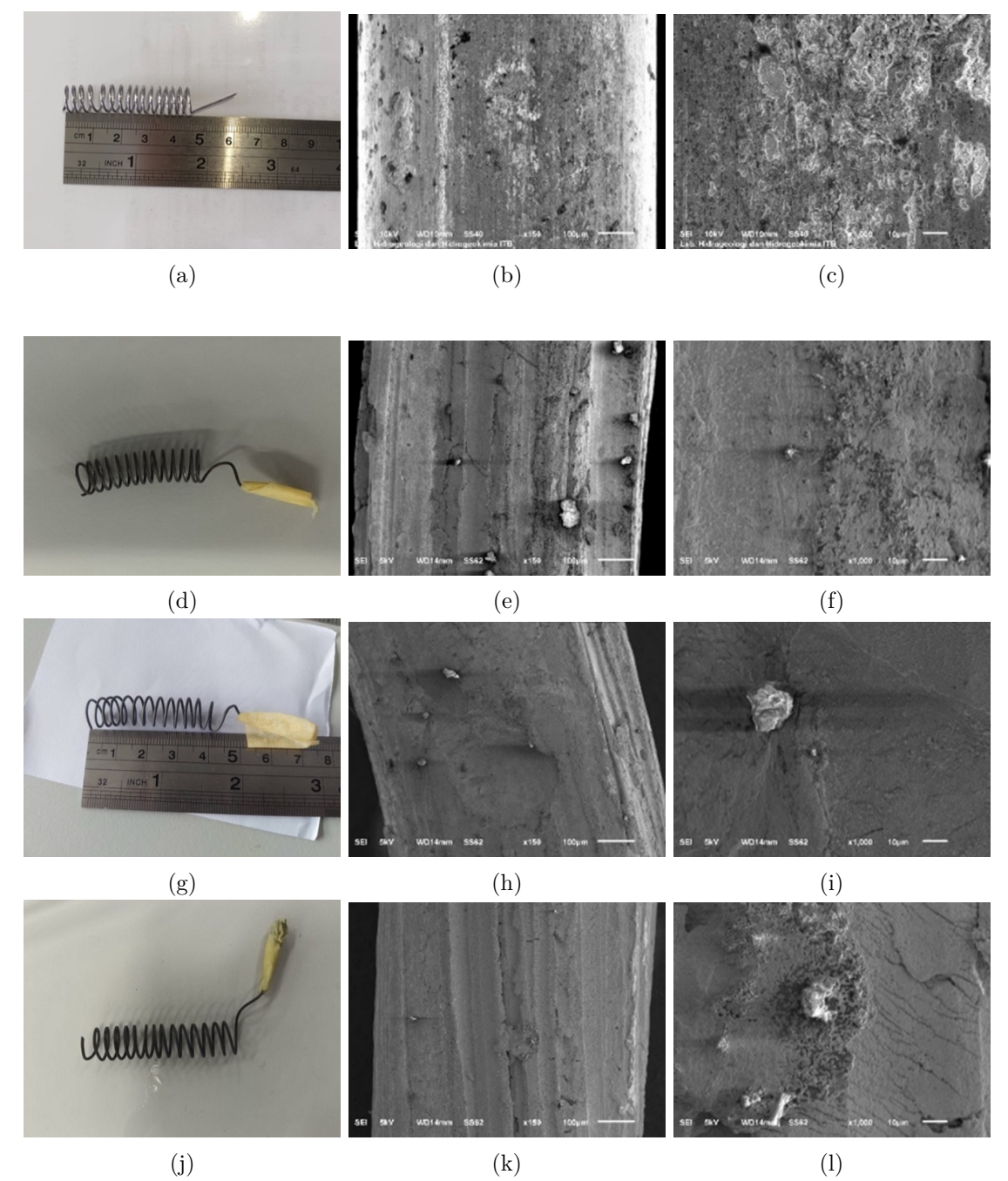


Figure 5 Scanning Electron Microscopy of the Pb-Sn cathode surface before use (a-c) and after electrochemical reduction of CO₂ using different sparger types: (d-f) bubble stone, (g-i) atomizer, and (j-l) air stone.

The XRD analysis presented in Figure 6 confirms the formation of SnO_2 layer on the cathode surface after electrolysis. The present of this oxide layer is believed to enhance the efficiency and stability of CO_2 electroreduction. Cathodes containing SnO_2 have been reported to exhibit higher partial current densities compared to other Sn -based catalysts (Duarah et al., 2021). Several studies have demonstrated the selective conversion of CO_2 to formic acid using SnO_2 , achieving Faradaic efficiency as high as 97% (Liang et al., 2018). The catalytic mechanism of SnO_2 in CO_2 electroreduction remains a subject of ongoing discussion. Choi et al. proposed that SnO_2 contributes to improved electrical conductivity and catalytic activity (Choi et al., 2016). In contrast, Salvini et al. using computational simulations, reported that the SnO_2 (110) surface itself does not actively involve in the catalytic process. Instead, under electrochemical conditions, SnO_2 undergoes partial reduction to form a bilayer structure composed of metallic tin atop the oxide surface (2 SnSnO_2), which is believed to be the active phase responsible for high selectivity

toward formic acid (Salvini et al., 2022). It is important to note that complete reduction of SnO_2 to metallic Sn shifts the selectivity toward hydrogen evolution, thereby reducing formic acid yield (T. Gao et al., 2019). Thus, maintaining a stable combination of Sn and SnO_2 phases is essential for optimizing yield, selectivity, and long-term stability of reaction. This observation aligns with our previous work, where the presence of SnO_2 contributed to stable performance over 7 hours of continuous operation (Widiatmoko et al., 2020).

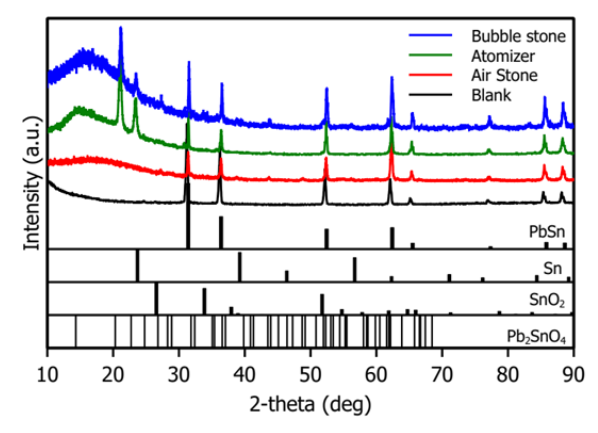


Figure 6 X-ray diffraction (XRD) patterns of the Pb-Sn cathode before use (blank) and after electrochemical CO₂ reduction using different sparger types: bubble stone, atomizer, and air stone. Reference patterns for PbSn, Sn, SnO₂, and Pb₂SnO₄ phases are also included for phase identification.

4. Conclusion

Smaller bubble size demonstrated superior performance in the electrochemical reduction of CO₂. The bubble stone sparger, which generates bubbles with diameters 6.18 and 3.26 times smaller than those produced by atomizer and air stone, respectively, resulted in 29.23% and 15.23% higher current efficiency. Correspondingly, the formic acid yield was 50.70% and 28.21% greater compared to the other sparger types under the same operating voltage. A shorter distance between the sparger and the cathode generally led to higher current efficiency and formic acid yield, and this trend was also consistently observed with shorter cathode across all experimental conditions. Future studies should further investigate the use of microbubbles and nanobubbles to determine the optimal bubble size range. Microbubbles may offer advantages due to their slower dissolution rates of CO₂, while nanobubbles could enhance reactivity through their high surface energy resulting from significant surface tension. Additionally, reactor design, particularly the distance between sparger and cathode, should be optimized, considering the low terminal velocity of micro- and nanobubbles, which may influence mass transfer and gas-liquid contact efficiency.

Acknowledgements

This research was funded by Riset Unggulan ITB 2022 Program No. contract FTI.PN-6-15-2022, 223/IT1.B07.1/TA.01/2022. We also thank Prof. Dr.Eng. I Made Joni, M.Sc. and team for kind support on this research.

Conflict of Interest

The authors declare no conflicts of interest in this research.

References

- Anggerta, L. A., Kurniawansyah, F., Tetrisyanda, R., & Wibawa, G. (2025). Catalytic Synthesis of Diethyl Carbonate from Carbon Dioxide using Catalyst KI/EtONa with Propylene Oxide as Dehydration Agent and Process Optimization Based on Box-Behnken Design. *International Journal of Technology*, 16(1), 243–254. https://doi.org/10.14716/ijtech.v16i1.6417
- Angulo, A., van der Linde, P., Gardeniers, H., Modestino, M., & Fernández Rivas, D. (2020). Influence of bubbles on the energy conversion efficiency of electrochemical reactors. *Joule*, 4(3), 555–579. https://doi.org/https://doi.org/10.1016/j.joule.2020.01.005
- Bagemihl, I., Bhatraju, C., van Ommen, J. R., & van Steijn, V. (2022). Electrochemical Reduction of CO2 in Tubular Flow Cells under Gas-Liquid Taylor Flow. ACS Sustainable Chemistry & Engineering, 10(38), 12580–12587. https://doi.org/10.1021/acssuschemeng.2c03038
- Bagotzky, V. S. (2006). Fundamentals of electrochemistry (2nd ed.). Wiley-Interscience.
- Bang, J.-H., Song, K., Park, S., Jeon, C., Lee, S. W., & Kim, W. (2015). Effects of CO2 Bubble Size, CO2 Flow Rate and Calcium Source on the Size and Specific Surface Area of CaCO3 Particles. *Energies*, 8(10), 12304–12313. https://doi.org/10.3390/en81012304
- Baumgartner, L. M., Kahn, A., Hoogland, M., Bleeker, J., Jager, W. F., & Vermaas, D. A. (2023). Direct Imaging of Local pH Reveals Bubble-Induced Mixing in a CO2 Electrolyzer. *ACS Sustainable Chemistry & Engineering*, 11(28), 10430–10440. https://doi.org/10.1021/acssuschemeng.3c01773
- Bulushev, D. A., & Ross, J. R. H. (2018). Towards Sustainable Production of Formic Acid. ChemSusChem, 11(5), 821–836. https://doi.org/10.1002/cssc.201702075
- Chang, B., Pang, H., Raziq, F., Wang, S., Huang, K.-W., Ye, J., & Zhang, H. (2023). Electrochemical reduction of carbon dioxide to multicarbon (C2+) products: Challenges and perspectives. *Energy & Environmental Science*, 16(11), 4714–4758. https://doi.org/10.1039/D3EE00964E
- Choi, S., Jeong, S., Kim, H., Baek, I.-H., & Park, K. (2016). Electrochemical reduction of carbon dioxide to formate on tin–lead alloys. *ACS Sustainable Chemistry & Engineering*, 4(3), 1311–1318. https://doi.org/10.1021/acssuschemeng.5b01336
- Daiyan, R., Lu, X., Ng, Y., & Amal, R. (2017). Liquid hydrocarbon production from CO2: Recent development in metal-based electrocatalysis. *ChemSusChem*, 10(22), 4342–4358. https://doi.org/10.1002/cssc.201701631
- Duarah, P., Haldar, D., Yadav, V., & Purkait, M. (2021). Progress in the electrochemical reduction of CO2 to formic acid: A review on current trends and future prospects. *Journal of Environmental Chemical Engineering*, 9(6), 106394. https://doi.org/10.1016/j.jece. 2021.106394
- Ewis, D., Arsalan, M., Khaled, M., Pant, D., Ba-Abbad, M., Amhamed, A., & El-Naas, M. (2023). Electrochemical reduction of CO2 into formate/formic acid: A review of cell design and operation. Separation and Purification Technology, 316, 123811. https://doi.org/10.1016/j.seppur.2023.123811
- Fan, L., Xia, C., Zhu, P., Lu, Y., & Wang, H. (2020). Electrochemical CO2 reduction to high-concentration pure formic acid solutions in an all-solid-state reactor. *Nature Communications*, 11(1), 3633. https://doi.org/10.1038/s41467-020-17403-1
- Fang, W., Guo, W., Lu, R., Yan, Y., Liu, X., Wu, D., Li, F., Zhou, Y., He, C., Xia, C., Niu, H., Wang, S., Liu, Y., Mao, Y., Zhang, C., You, B., Pang, Y., Duan, L., Yang, X., ... Xia, B. (2024). Durable CO2 conversion in the proton-exchange membrane system. *Nature*, 626 (7997), 86–91. https://doi.org/10.1038/s41586-023-06917-5
- Gao, G., Obasanjo, C., Crane, J., & Dinh, C.-T. (2023). Comparative analysis of electrolyzers for electrochemical carbon dioxide conversion. *Catalysis Today*, 423, 114284. https://doi.org/10.1016/j.cattod.2023.114284

- Gao, T., Kumar, A., Shang, Z., Duan, X., Wang, H., Wang, S., Ji, S., Yan, D., Luo, L., Liu, W., & Sun, X. (2019). Promoting electrochemical conversion of CO2 to formate with rich oxygen vacancies in nanoporous tin oxides. *Chinese Chemical Letters*, 30(12), 2274–2278. https://doi.org/10.1016/j.cclet.2019.07.028
- García, H., & Mejia, N. (2021). Mathematical model of a bubble column for the increased growth of Arthrospira platensis and the formation of phycocyanin. *International Journal of Technology*, 12(2), 232. https://doi.org/10.14716/ijtech.v12i2.4256
- Gemello, L., Plais, C., Augier, F., Cloupet, A., & Marchisio, D. (2018). Hydrodynamics and bubble size in bubble columns: Effects of contaminants and spargers. *Chemical Engineering Science*, 184, 93–102. https://doi.org/10.1016/j.ces.2018.03.040
- Hadi, I., Yola, L., Hanifa, A., & Muzhaffar, M. (2025). Decarbonization strategy towards net zero emission for international shipping on international shipping routes in indonesian archipelago sea lanes. *International Journal of Technology*, 16(1), 8. https://doi.org/10. 14716/ijtech.v16i1.7106
- Institute for Essential Services Reform. (2021). Climate transparency report 2021: Real climate change impacts, indonesia needs to increase its climate action [Accessed 8 August 2024]. https://iesr.or.id/en/climate-transparency-report-2021-real-climate-change-impacts-indonesia-needs-to-increase-its-climate-action/
- International Energy Agency. (2024). CO2 emissions in 2023, a new record high, but is there light at the end of the tunnel?
- Irabien, A., Alvarez-Guerra, M., Albo, J., & Dominguez-Ramos, A. (2018). Electrochemical conversion of CO2 to value-added products. In *Electrochemical water and wastewater treatment* (pp. 29–59). Elsevier. https://doi.org/10.1016/B978-0-12-813160-2.00002-X
- Jia, S., Ma, X., Sun, X., & Han, B. (2022). Electrochemical transformation of CO2 to value-added chemicals and fuels. CCS Chemistry, 4(10), 3213–3229. https://doi.org/10.31635/ccschem.022.202202094
- Kartohardjono, S., Karamah, E., Hayati, A., Talenta, G., Ghazali, T., & Lau, W. (2024). Effect of oxidants in the utilization of polysulfone hollow fiber membrane module as bubble reactor for simultaneously removal of NOx and SO2. *International Journal of Technology*, 15(1), 63. https://doi.org/10.14716/ijtech.v15i1.6415
- Kim, B., Ma, S., Molly Jhong, H.-R., & Kenis, P. (2015). Influence of dilute feed and pH on electrochemical reduction of CO2 to CO on Ag in a continuous flow electrolyzer. *Electrochimica Acta*, 166, 271–276. https://doi.org/10.1016/j.electacta.2015.03.064
- Kumar, B., Llorente, M., Froehlich, J., Dang, T., Sathrum, A., & Kubiak, C. (2012). Photochemical and photoelectrochemical reduction of CO2. *Annual Review of Physical Chemistry*, 63(1), 541–569. https://doi.org/10.1146/annurev-physchem-032511-143759
- Liang, C., Kim, B., Yang, S., Liu, Y., Woellner, C., Li, Z., Vajtai, R., Yang, W., Wu, J., Kenis, P., & Ajayan, P. (2018). High efficiency electrochemical reduction of CO2 beyond the two-electron transfer pathway on grain boundary rich ultra-small SnO2 nanoparticles. Journal of Materials Chemistry A, 6(22), 10313–10319. https://doi.org/10.1039/C8TA01367E
- Lin, R., Guo, J., Li, X., Patel, P., & Seifitokaldani, A. (2020). Electrochemical reactors for CO2 conversion. *Catalysts*, 10(5), 473. https://doi.org/10.3390/catal10050473
- Liu, C., & Tang, Y. (2019). Application research of micro and nano bubbles in water pollution control. E3S Web of Conferences, 136, 06028. https://doi.org/10.1051/e3sconf/201913606028
- Madani, H., Wibowo, A., Sasongko, D., Miyamoto, M., Uemiya, S., & Budhi, Y. (2024). Novel multiphase CO2 photocatalysis system using N-TiO2/CNCs and CO2 nanobubble. *International Journal of Technology*, 15(2), 432. https://doi.org/10.14716/ijtech.v15i2.6694
- Marcandalli, G., Monteiro, M., Goyal, A., & Koper, M. (2022). Electrolyte effects on CO2 electrochemical reduction to CO. *Accounts of Chemical Research*, 55(14), 1900–1911. https://doi.org/10.1021/acs.accounts.2c00080

- Moret, S., Dyson, P., & Laurenczy, G. (2014). Direct synthesis of formic acid from carbon dioxide by hydrogenation in acidic media. *Nature Communications*, 5(1), 4017. https://doi.org/10.1038/ncomms5017
- Moshtari, B., Babakhani, E., & Moghaddas, J. (2009). Experimental study of gas hold-up and bubble behaviour in gas-liquid column [No available DOI].
- Mudassir, R. (2021). Bauran energi, porsi pembangkit EBT tembus 12,77 persen [Accessed 8 August 2024]. https://ekonomi.bisnis.com/read/20211021/44/1456788/bauran-energi-porsi-pembangkit-ebt-tembus-1277-persen
- Popov, K., Djokic, S., & Grgur, B. (2005). Fundamental aspects of electrometallurgy. Kluwer Academic/Plenum Publishers.
- Ramadhan, R., Mon, M., Tangparitkul, S., Tansuchat, R., & Agustin, D. (2024). Carbon capture, utilization, and storage in indonesia: An update on storage capacity, current status, economic viability, and policy. *Energy Geoscience*, 5(4), 100335. https://doi.org/10.1016/j.engeos.2024.100335
- Sacco, A., Zeng, J., Bejtka, K., & Chiodoni, A. (2019). Modeling of gas bubble-induced mass transport in the electrochemical reduction of carbon dioxide on nanostructured electrodes. *Journal of Catalysis*, 372, 39–48. https://doi.org/10.1016/j.jcat.2019.02.016
- Salvini, C., Re Fiorentin, M., Risplendi, F., Raffone, F., & Cicero, G. (2022). Active surface structure of SnO2 catalysts for CO2 reduction revealed by Ab Initio simulations. *The Journal of Physical Chemistry C*, 126(34), 14441–14447. https://doi.org/10.1021/acs.jpcc.2c02583
- Suwartha, N., Syamzida, D., Priadi, C., Moersidik, S., & Ali, F. (2020). Effect of size variation on microbubble mass transfer coefficient in flotation and aeration processes. *Heliyon*, 6(4), e03748. https://doi.org/10.1016/j.heliyon.2020.e03748
- Temesgen, T., Bui, T., Han, M., Kim, T., & Park, H. (2017). Micro and nanobubble technologies as a new horizon for water-treatment techniques: A review. Advances in Colloid and Interface Science, 246, 40–51. https://doi.org/10.1016/j.cis.2017.06.011
- The International Renewable Energy Agency. (2022). Indonesia energy transition outlook.
- Wang, X., Meng, Q., Gao, L., Jin, Z., Ge, J., Liu, C., & Xing, W. (2018). Recent progress in hydrogen production from formic acid decomposition. *International Journal of Hydrogen Energy*, 43(14), 7055–7071. https://doi.org/10.1016/j.ijhydene.2018.02.146
- Whulanza, Y., Kusrini, E., Budiyanto, M., Arnas, A., & Yanuar, Y. (2024). Decarbonizing the maritime industry: A collaborative path forward. *International Journal of Technology*, 15(6), 1593. https://doi.org/10.14716/ijtech.v15i6.7526
- Widiatmoko, P., Hendra Saputera, W., Devianto, H., Nurdin, I., Rivana, E., & Angkasa, A. (2021). Effect of bubble size on electrochemical reduction of carbon dioxide to formic acid. *IOP Conference Series: Materials Science and Engineering*, 1143(1), 012001. https://doi.org/10.1088/1757-899X/1143/1/012001
- Widiatmoko, P., Nurdin, I., Devianto, H., Prakarsa, B., & Hudoyo, H. (2020). Electrochemical reduction of CO2 to formic acid on Pb-Sn alloy cathode. *IOP Conference Series:*Materials Science and Engineering, 823(1), 012053. https://doi.org/10.1088/1757-899X/823/1/012053
- Wu, J., Risalvato, F., & Zhou, X.-D. (2012). Effects of the electrolyte on electrochemical reduction of CO2 on Sn electrode. ECS Transactions, 41(33), 49–60. https://doi.org/10.1149/1.3702412
- Zhao, J., Liu, Y., Li, W., Wen, C., Fu, H., Yuan, H., Liu, P., & Yang, H. (2023). A focus on the electrolyte: Realizing CO2 electroreduction from aqueous solution to pure water. *Chem Catalysis*, 3(1), 100471. https://doi.org/10.1016/j.checat.2022.11.010
- Zhong, H., Fujii, K., & Nakano, Y. (2017). Effect of KHCO3 concentration on electrochemical reduction of CO2 on copper electrode. *Journal of The Electrochemical Society*, 164(9), F923–F927. https://doi.org/10.1149/2.0601709jes

Zhong, H., Fujii, K., Nakano, Y., & Jin, F. (2015). Effect of CO2 bubbling into aqueous solutions used for electrochemical reduction of CO2 for energy conversion and storage. *The Journal of Physical Chemistry C*, 119(1), 55–61. https://doi.org/10.1021/jp509043h